NASA Technical Memorandum 86389

Nozzle Wall Roughness Effects on Free-Stream Noise and Transition in the Pilot Low-Disturbance Tunnel

Theodore R. Creel, Jr., and Ivan E. Beckwith
Langley Research Center
Hampton, Virginia

Fang-Jenq Chen
High Technology Corporation
Hampton, Virginia

National Aeronautics
and Space Administration

**Scientific and Technical
Information Branch**

1985

1. Report No.	2. Government Accession No.	3. Recipient's Catalog No.
NASA TM-86389		

4. Title and Subtitle	5. Report Date
Nozzle Wall Roughness Effects on Free-Stream Noise and Transition in the Pilot Low-Disturbance Tunnel	September 1985
	6. Performing Organization Code 505-31-13-06
7. Author(s) Theodore R. Creel, Jr., Ivan E. Beckwith, and Fang-Jenq Chen	8. Performing Organization Report No. L-15903
	10. Work Unit No.
9. Performing Organization Name and Address NASA Langley Research Center Hampton, VA 23665	11. Contract or Grant No.
	13. Type of Report and Period Covered Technical Memorandum
12. Sponsoring Agency Name and Address National Aeronautics and Space Administration Washington, DC 20546	14. Sponsoring Agency Code

15. Supplementary Notes

Theodore R. Creel, Jr., and Ivan E. Beckwith: NASA Langley Research Center, Hampton, Virginia.
Fang-Jenq Chen: High Technology Corporation, Hampton, Virginia.

16. Abstract

An investigation at Mach 3.5 into the effects of nozzle wall roughness on free-stream pressure fluctuations and cone transition Reynolds numbers was conducted in the pilot low-disturbance tunnel at the Langley Research Center. Nozzle wall roughness caused by either particle deposits or imperfections in surface finish increased free-stream noise levels and reduced the transition Reynolds numbers on a cone mounted in the test rhombus.

17. Key Words (Suggested by Author(s))	18. Distribution Statement
Boundary-layer transition Free-stream noise Supersonic wind tunnel	Unclassified - Unlimited Subject Category 34

19. Security Classif. (of this report)	20. Security Classif. (of this page)	21. No. of Pages	22. Price
Unclassified	Unclassified	32	A03

For sale by the National Technical Information Service, Springfield, Virginia 22161

SUMMARY

The influence of nozzle wall roughness on free-stream pressure fluctuations and cone transition Reynolds numbers in the pilot low-disturbance tunnel at the Langley Research Center was studied. Nozzle wall roughness caused by particulate deposits or by machining imperfections increased free-stream noise levels either by creating shimmering Mach waves or by tripping the nozzle wall boundary layer. These increased noise levels reduced transition Reynolds numbers on a cone mounted in the test rhombus.

INTRODUCTION

Problems related to air filters and the effects of contaminant wall deposits on tunnel flow quality have been encountered in the Mach 3.5 pilot low-disturbance tunnel at the Langley Research Center (refs. 1 to 3). To obtain the low-disturbance environment in the tunnel test section which is required for transition research, stream disturbances must be reduced to an acceptable level. Kovásznay (ref. 4) showed that there are three basic types of free-stream disturbances: (1) vorticity fluctuations, (2) entropy fluctuations, and (3) pressure fluctuations or acoustic disturbances.

Vorticity fluctuations are generally reduced to negligible values by the use of a large contraction ratio. Previous research (refs. 5 to 7) indicated that in a well-designed wind tunnel, for Mach numbers (M) greater than 2.5, vorticity fluctuations were too small to affect transition data. However, hot-wire and fluctuating pitot pressure data obtained in the Nozzle Test Chamber at Langley Research Center (ref. 8) indicated that large settling chamber disturbances were not adequately damped as the flow accelerated through the contraction into the nozzle. Stainback and Wagner (ref. 8) noted that higher transition Reynolds numbers were obtained on a test cone when there were no screens or flow conditioner devices in the settling chamber than when such devices were in place. When screens were added to the settling chamber, they increased free-stream flow disturbance levels and decreased transition Reynolds numbers. The stated reasons (ref. 8) for this apparent anomaly were the leakage of air around the screen support rings and the short distance from the screens to the throat for the streamwise decay of vorticity. Reference 9 described examples of satisfactory settling chamber design in which the rms velocity fluctuation levels in the settling chamber were reduced to 1 percent or less, and the rms fluctuation pressure (noise) levels were reduced to 0.01 percent; both levels were required to insure high-quality flow in the test section for Mach numbers below 3 and at high test Reynolds numbers. At higher Mach numbers, the vorticity levels are not as critical (ref. 6), but the noise levels should always be reduced as much as possible.

Entropy fluctuations may be reduced if the test medium is thoroughly mixed in the tunnel settling chamber. In the pilot low-disturbance tunnel, the porous plates and steel wool, which are used primarily to reduce the control valve and pipe noise (ref. 9), also function as good flow mixers. Thus, with two of the three free-stream disturbance modes reduced to acceptable levels, our current research effort focused on reducing or eliminating the stream pressure fluctuation or acoustic disturbance mode.

In 1959, Morkovin (ref. 10) discussed four possible types of acoustic disturbances in supersonic wind tunnels. These disturbances are: (1) acoustic disturbances transmitted into the test section from the settling chamber (e.g., pipe and control valve noise), (2) aerodynamic noise radiation (eddy Mach wave noise radiation) from moving sources within the turbulent boundary layers on the nozzle wall, (3) "shivering" Mach waves from fixed sources such as nozzle wall waviness and roughness, and (4) wall vibrations. These sources are present to some extent in most conventional wind tunnels.

Wall vibrations (acoustic disturbance type (4)) are usually not a problem in supersonic wind tunnels because the structural components are generally too massive to be excited at the high frequencies (>10 kHz) of concern. As mentioned previously, the pipe and control valve noise (acoustic disturbance type (1)) in the pilot low-disturbance tunnel was reduced to very low levels by porous plates in the settling chamber (ref. 9). Data gathered in the pilot low-disturbance tunnel from hot-wire and pressure-transducer probes (refs. 1 to 3) indicated that the eddy Mach wave radiation (acoustic disturbance type (2)) was eliminated in upstream regions of the test rhombus up to a free-stream Reynolds number of 8×10^5 per inch when laminar boundary layers were maintained on the nozzle walls through the corresponding acoustic origin locations.

Any possible effects of the one remaining type of acoustic disturbance discussed by Morkovin (ref. 10), i.e., the shivering or "shimmering" Mach waves (type 3), have not been reported for the Mach 3.5 pilot low-disturbance tunnel (refs. 1 to 3). Shimmering Mach waves may be caused by the reflection and scattering of steady disturbances from the turbulent boundary layers on the nozzle wall, or by disturbances caused by nozzle wall waviness or roughness which are then shimmered by interaction with the turbulent boundary layer (ref. 10). The reflection and scattering of steady disturbances from the nozzle wall boundary layer is not a significant problem in the present Mach 3.5 nozzle because the nozzle has a very rapid expansion contour and is therefore too short for reflections from upstream sources to be present in the quiet test region. Wall roughness can be reduced by improved machining and polishing procedures. Some limited experimental results from the Mach 3.5 pilot low-disturbance tunnel concerning the influence of nozzle wall finish on free-stream noise and transition on a test cone are presented in this paper. The problem of dust and other contaminant deposits on the nozzle wall is also considered. Contaminant deposits and the wall roughness can increase stream noise either by tripping the nozzle wall boundary layer or by creating shimmering Mach waves.

SYMBOLS

M	Mach number
P	pressure
R	unit Reynolds number, $\rho u/\mu$
$R_{e,T}$	local transition Reynolds number based on flow length from cone apex
rms	root-mean-square
u	streamwise velocity
X	axial distance from nozzle throat

Δ increment

μ dynamic viscosity

ρ mass density

Subscripts:

c cone apex

e local values at boundary-layer edge

T onset of transition

t pitot pressure probe

∞ free-stream static conditions

Superscripts:

~ root-mean-square

- mean value

APPARATUS

Facility

The pilot low-disturbance tunnel is located in the Gas Dynamics Laboratory at the Langley Research Center. The settling chamber is approximately 21 ft long with a 2-ft inside diameter and contains seven turbulence screens plus several dense porous plates that function as acoustic baffles to attenuate the high-level noise from the upstream control valves and high-pressure piping system (ref. 9). The facility utilizes a Mach 3.5 nozzle (shown in fig. 1); the nozzle dimensions are given in figure 1(a). Figure 1(b) is a photograph of the subsonic approach, which provides a smooth transition from the circular section of the settling chamber to the boundary-layer removal slots and the rectangular throat. Airflow through the slots is controlled by a valve, referred to herein as the bleed valve. When the bleed valve is open, the wall boundary-layer flow is laminar for different distances downstream of the throat depending on the value of R_∞. When the bleed valve is closed, the wall boundary-layer flow is turbulent except at the lowest value of R_∞. A more complete description of the settling chamber, nozzle, and test section can be found in references 1 to 3.

Air Supply System

The high-pressure air system, which consists of the compressors, dryers, storage tanks, heater, and filters that reduce the solid contaminants in the air, is necessary to the operation of the tunnel. Figure 2 is a highly simplified sketch of the arrangement of these components. During normal operation of the air supply system, air is pumped to a maximum pressure of 4200 psia by a six-stage compressor. The high pressure condenses most of the water vapor, which is removed by interstage condensers

and the 20-μm aerosol filter. The air is then dried further to a dewpoint of -40°F (measured at atmospheric pressure) by desiccant-type dryers using pelletized activated alumina oxide as the drying agent. The pellets, which have a powdery coating in their original condition, have a tendency to disintegrate after repeated usage because of physical abrasion and water saturation. Most of the powder and the larger particles of alumina oxide are removed by the 10-μm dust filter located downstream of the dryers. Unfortunately, some components of the system are regularly exposed to atmospheric air and occasionally to flooding for hydrostatic pressure tests. The resulting problem of rust throughout the system has been observed and is discussed in the Contaminant Samples section of this paper.

Filters

Because a superfinish on the nozzle walls and models is required for laminar nozzle wall flow and flight-valid facility transition data, an extremely clean air supply must be provided. Additional filters are required, and mesh-type filter elements were chosen for this application. As shown in figure 2, two different filters (40 μm and 1 μm) are used downstream of the storage bottles. The first in-line downstream filter has a fibrous-type element that is rated as a 40-μm filter.

Sectional drawings of the last in-line downstream filter (as modified from the original configuration) are shown in figure 3. This filter is located just upstream of the tunnel. The filter housing is designed for 800 psig and a temperature range of 0°F to 400°F. The inlet air flows through 14 filter elements mounted on the internal support structure, as indicated in figures 3(a) and 3(b).

The filter elements originally used were rated at 95 percent efficiency for the removal of 0.6-μm particles. The original elements were composed of a 1/8-in-thick mat of borosilicate microfibers. Problems occurred during the operation of the tunnel with these fibrous filter elements; the most frequent failure mode was element rupture.

During the investigation of the filter-element failures, it was found that some of the elements were bent in the direction of the airflow. The aerodynamic loads on a filter element were estimated to be 9 lb. A test indicated that a 10-lb force was sufficient to bend the elements 1/2 in. to 1 in. from a perpendicular direction at the element top; a 20-lb pull was sufficient to cause a 2-in. to 3-in. permanent deflection of the elements. This deflection allowed air to bypass the elements and resulted in dirty air entering the tunnel. The solution to this problem was to use a plate (fig. 4) to hold the element tops in position.

The solution to the fibrous filter-element rupture was to install sintered porous stainless-steel filter elements (fig. 5(a)) which are rated by the manufacturer to remove 99.5 percent of all particles greater than 1 μm in size. These elements were designed for a maximum drop in working pressure of 100 psid.

An additional problem occurred because the original inside-out flow through the elements (fig. 3(a)) caused the flat rubber gaskets (fig. 5(a)) to blow out. The solution was to rotate the filter case so that the flow through the elements was from outside to inside.

Further operating experience with the stainless-steel filter elements showed that some contaminants still bypassed the flat gaskets and were carried into the settling chamber. Figure 4 is a set of photographs taken after a series of tunnel

runs. The filter elements had been cleaned before this series of runs and had the characteristic steel-grey color of clean stainless steel. As shown in figure 4, the elements exhibit a variation of color starting with an extremely light brown in the center areas and gradually darkening until at the ends the elements are completely brown. A laboratory analysis of particulate samples presented in the Results and Discussion section of this report indicated that this brown material was iron oxide.

Both the top and the bottom of the filter elements collected dust. Inspection of the flat gaskets (fig. 5(a)) indicated that air and contaminants were leaking past the gaskets. These gaskets were then replaced with O-ring seals (fig. 5(b)). The O-ring seal arrangement proved to be effective in reducing the bypass leaks of contaminated air which occurred with the original flat gaskets. However, mechanical problems with the removal and reinstallation of the 14-element array after the frequent cleaning operations necessary to maintain $\Delta P \leq 75$ psid, motivated the new design illustrated in figure 5(c). This design eliminated all possible leak paths except the pipe thread fitting at the base of the elements; this fitting has not caused any problems to date.

Instrumentation

Hot-wire data were obtained over a range of stagnation pressures from about 25 psia to 150 psia at stagnation temperatures from about 60°F to 85°F by using a constant-current anemometer with an automatic overheat switching circuit. Data presented in this report were taken with a Datametrics Model 1900-1 anemometer. The anemometer and operating procedures are described in references 1 and 2. Fluctuating pitot pressures were measured with miniature high-frequency-response strain-gage type-transducers used as pitot probes (ref. 3).

Models

Transition Reynolds numbers were obtained on two sharp-apex 5° half-angle stainless-steel cones. These transition data were obtained from recovery temperature measurements made with 0.010-in-diameter thermocouples installed in or spot welded to the 0.03 in-thick thin-skin wall. The first cone is described in reference 1 and is designated herein as cone 1. The surface finish of cone 1 could not be maintained in good condition for all the tests because the thermocouples occasionally worked loose and extended above the cone surface. The junction between the nose tip and cone body was also not perfectly flush. Therefore, a second stainless-steel cone of the same size as cone 1 was constructed. The major differences between this cone, designated cone 2, and cone 1 are given below.

1. The thermocouples of cone 1 were soft soldered into 0.025-in-diameter holes drilled through the 0.03-in-thick skin. The thermocouples of cone 2 were spot welded to the inside surface of the 0.03-in-thick skin.

2. The junction of the nose tip and cone body and the overall surface finish of cone 2 were much better than those of cone 1. According to sample profilometer records the final surface finish on cone 2 was 1 μin. to 2 μin. and the maximum peak-to-valley roughness was 12 μin. Unfortunately, due to a defect in the junction (at 1 in. from the cone apex) between the tip piece and the cone frustrum, a new tip had to be made. After the installation of this new tip and the final polishing of the cone were completed, additional profilometer records were not obtained. However, visual

inspection indicated that the finish on cone 2 with the new tip was as good as that of the original cone 2.

RESULTS AND DISCUSSION

Contaminant Samples

Contaminant samples were collected on 1-in-diameter flat-face cylinders coated with an oily film or wax so that particles adhered to the surface. Samples of contaminants or dust collected in the pilot low-disturbance tunnel before the Mach 3.5 nozzle or the stainless-steel filter elements were installed are shown in figure 6. A laboratory analysis of the samples indicated that six different types of contaminants entered the tunnel. Because the samples were not photographed in color, only two of these samples are shown in figure 6. The six different types of contaminants were:

(1) Black dust (fig. 6(a)), size range 0.36 mm to 6 μm; iron particles

(2) Yellow or rust-colored dust, 0.36 mm to 6 μm; iron oxide

(3) White dust, ≤5 μm; alumina oxide

(4) Small fibers (fig. 6(b)), ≤5 μm; presumably from original fibrous filter elements

(5) Larger fibers; semitransparent, irregularly shaped, probably from clothing, tissue, and paper fibers

(6) Miscellaneous; red fiber (probably nylon), animal or human hair (according to the visible scale pattern), a few diatoms, and pollen spores

This laboratory analysis included a test that confirmed the presence of iron oxide. This iron oxide was probably from the carbon steel piping system, which for the purpose of hydrostatic tests had been subjected to water incursions several times. The elimination of rust and other particles from the free stream of the pilot low-disturbance tunnel is of extreme importance. Reference 11 pointed out that extremely small particles, such as dust motes, caused transition in the boundary layer on a rotating disk. The experiment (ref. 11) was performed on a rotating disk at atmospheric conditions and subsonic speeds. If dust particles settle on the nozzle surface of a supersonic tunnel where the boundary layer is very thin (about 0.002 in. thick in the nozzle throat region at R_∞ per inch $\approx 8 \times 10^5$), these particles can cause transition and/or shimmering Mach waves.

Under normal circumstances, the pilot low-disturbance tunnel is open to the dust-contaminated atmosphere during model changes and test section modification. Some method should be devised to prevent room air from entering the test section. This method could include pressurizing the tunnel system to some fractional psi so that a positive airflow out of the tunnel would occur at any time the test section doors or the tunnel were open to the atmosphere. This pressurization should include the settling chamber, the nozzle, the test section, and enough of the piping system downstream of the test section so that there would not be any backflow of contaminated air into the nozzle.

Noise Measurements

Figure 7 presents typical data sets for the normalized rms static pressure (noise) obtained from axial surveys with hot-wire probes along the nozzle centerline. The bleed valve was open and the nozzle wall was either "clean" or "dirty" over the Reynolds number ranges given in the figure. In the present report, the clean condition was obtained by carefully cleaning the nozzle walls with lint-free material and alcohol just before a data run. The walls were then vacuumed to remove residual atmospheric dust and lint. This procedure was always required to obtain the best results. The dirty condition occurred due to the nozzle walls that were not cleaned for several previous runs and visible deposits of lint, dust, or other types of contaminants that were present before a run. This dirty condition was especially prevalent during the earlier tests (refs. 1 to 3) due to chronic problems with seals on the 1-μm air filter elements and the resulting residual contamination in the settling chamber and entrance pipes. Recent improvements in the air filter system, as described previously, have reduced the contamination problems, but periodic cleaning of the nozzle surfaces is still required.

When the values of $\tilde{P}/\bar{P}$ were less than 0.1 percent, the nozzle wall boundary layer was laminar at the acoustic origins, and the signal levels were so close to the instrument noise levels that the data were not considered reliable (refs. 1 and 2). Nevertheless, a useful criterion for the location of transition has been established (and verified by the spectral data, ref. 1) as the value of X where a faired curve for $\tilde{P}/\bar{P}$ increases above 0.1 percent. Application of this criterion to the data in figure 7 showed that the dust deposits caused transition to move about 1/2 in. to 2 1/2-in. (as measured on the nozzle centerline) upstream of the location for the clean-wall condition. This movement, however, depended on the unit Reynolds number. Downstream of transition, the noise levels were always higher when dust deposits were present. These higher noise levels presumably were due to shimmering Mach waves that originated from the dust particles. At the highest unit Reynolds number ($R_\infty = 12 \times 10^{-5}$ per inch) the nozzle wall boundary layers at the corresponding acoustic origin locations (ref. 1) were turbulent for $X > 5$ in., and again the noise levels were always higher when dust deposits were present.

The initial experiments were not intended to precisely quantify the dust particle roughness effects, and therefore this aspect of the problem is not as complete as it should be. More extensive tests are needed to better define the effects on the free stream noise of roughness particles with known sizes and distributions.

Effect of Nozzle Wall Deposits on Cone Transition Reynolds Numbers

In order to further investigate the effects of contamination, transition Reynolds numbers for cone 1 with the nozzle walls clean and dirty, with the bleed valve open, and with $X_c = 8$ in. are presented in figure 8. Wall deposit effects were not apparent for $R_e = 4.8 \times 10^5$ per inch. At this value of R_e, the upstream part of the cone was located in a region of the nozzle test core where the nozzle boundary layers at the acoustic origins were laminar and the noise incident on the cone tip region was small (refs. 1 and 2). As the Reynolds number increased ($R_e > 6.8 \times 10^5$ per inch), the values of $R_{e,T}$ for the cone when the nozzle wall was dirty decreased below the values for the clean condition. This decrease was caused either by dirt particles that adhered to the nozzle walls and created shimmering Mach waves that impinged on the cone boundary layer, or, for $R_\infty < 1 \times 10^6$ per inch, by dust particles that caused the boundary-layer transition to move farther upstream on the nozzle walls (fig. 7). In either of these situations, higher noise levels were

present outside the boundary layer on the cone and the dust deposits had significant adverse effects on transition on the test cone.

Effects of Nozzle Wall Roughness

The data in the previous discussion were obtained when the nozzle wall had a good surface finish. However, repeated usage, frequent cleaning of the nozzle, and the degradation of the surface finish caused by many runs with some leakage of particles through the filter required that the nozzle be repolished.

Surface finish.- Repolishing improved the nozzle surface finish substantially, as shown in figure 9, which shows representative traces of the actual profilometer readings taken before (fig. 9(a)) and after repolishing (fig. 9(b)). Additional profilometer data are given in table I. This table presents data taken before and after the repolishing work on the two nozzle blocks at five different axial and lateral locations in the upstream regions of the nozzle. Values in microinches for typical ranges and maximum local deviations for both rms finish and the roughness (in terms of peak-to-valley distances) are listed in the table. The second line for each location gives the data after the repolishing work was completed. In all cases, a significant reduction occurred in both the rms and peak-to-valley profilometer readings as a result of the repolishing work.

Noise data.- Figure 10 presents noise data measured on the nozzle centerline before (fig. 10(a)) and after repolishing (fig. 10(b)). The corresponding values of X_T on the centerline and the nozzle wall are included for comparison. Unfortunately, the data were obtained with two different techniques (hot-wire anemometer and fluctuating pitot pressure transducer), so the noise levels are somewhat different. However, for our purpose, we are concerned only with significant changes in the location of transition (defined herein as the value of X where a faired curve through the noise data crosses the value $\tilde{P}_\infty/\bar{P}_\infty = 0.1$ percent). Comparisons of data from the two techniques before the nozzle was repolished (ref. 1) indicate that the X_T values were in reasonable agreement. Hence, it is concluded that the repolishing operation resulted in significantly longer runs of laminar flow in the nozzle wall boundary layer.

Transition on a test cone.- Figure 11 shows the effect of repolishing the nozzle walls on transition Reynolds numbers on cone 2. With the bleed valve open (fig. 11(a)) and for $R_\infty \approx 1.0 \times 10^6$ per inch, $R_{e,T}$ increased from about 4.5×10^6 to 8.0×10^6 as a result of the improved finish (table I and fig. 10) achieved by the repolishing operation. The scatter in both sets of data increases as R_∞ increases above 1.0×10^6 per inch.

Examination of the individual run records indicated that the lower values of $R_{e,T}$ for these larger unit Reynolds numbers both before and after repolishing could usually be attributed to contamination of the nozzle surface due to leaks in the air filter seals (data of ref. 1) or residual and atmospheric contamination (data reported herein). In any event, very good surface finishes on the nozzle walls were required to obtain transition Reynolds numbers approaching flight data on a test model in this pilot nozzle when $R_\infty > 8 \times 10^5$ per inch. These large values of $R_{e,T}$ are attributed to the longer runs of laminar flow on the nozzle wall (as indicated by the data in fig. 10).

In order to determine whether the nozzle wall surface finish or the improved surface finish of cone 2 over that of cone 1 was the cause of the high transition

Reynolds numbers with the bleed valve open (fig. 11(a)), cone 2 was also tested with the bleed valve closed (fig. 11(b)). When the bleed valve was closed, the nozzle wall boundary layers for $R_\infty > 7.5 \times 10^5$ per inch were completely turbulent, and the noise levels ranged from about 0.2 to 0.4 percent with large energy levels at high frequencies (ref. 1). With these higher noise conditions, transition Reynolds numbers for cone 2 were of the same order or even lower than the values obtained on cone 1. Hence, it may be concluded that the main cause of both the higher values of $R_{e,T}$ obtained with the bleed valve open and the corresponding low noise levels was the improved nozzle finish and not the better surface finish of cone 2.

CONCLUDING REMARKS

The effects of solid-particle contaminant deposits on the nozzle wall were investigated by obtaining free-stream fluctuation pressures and transition Reynolds numbers on the surface of a sharp-apex 5° half-angle cone in a Mach 3.5 nozzle over a unit Reynolds number range from 2.5×10^5 per inch to 15×10^5 per inch. These data showed that contaminant deposits caused increases in free-stream noise levels because they acted as boundary-layer trips on the nozzle wall at low test Reynolds numbers. At high test Reynolds numbers, the particle deposits increased the noise levels by increasing shimmering Mach wave noise from fixed sources on the walls. Increased free-stream noise levels in turn caused low transition Reynolds numbers on a cone model in the test core. Nozzle surface roughness also had large adverse effects on free-stream noise and transition Reynolds numbers on the cone.

NASA Langley Research Center
Hampton, VA 23665
May 1, 1985

REFERENCES

1. Beckwith, Ivan E.; Creel, Theodore R., Jr.; Chen, Fang-Jenq; and Kendall, James M.: Free-Stream Noise and Transition Measurements on a Cone in a Mach 3.5 Pilot Low-Disturbance Tunnel. NASA TP-2180, 1983.

2. Beckwith, Ivan E.; Creel, Theodore R., Jr.; Chen, Fang-Jenq; and Kendall, James M.: Free Stream Noise and Transition Measurements in a Mach 3.5 Pilot Quiet Tunnel. AIAA-83-0042, Jan. 1983.

3. Beckwith, Ivan E.; and Moore, William O., III: Mean Flow and Noise Measurements in a Mach 3.5 Pilot Quiet Tunnel. A Collection of Technical Papers - AIAA 12th Aerodynamic Testing Conference, Mar. 1982, pp. 48-70. (Available as AIAA-82-0569.)

4. Kovásznay, Leslie S. G.: Turbulence in Supersonic Flow. J. Aeronaut. Sci., vol. 20, no. 10, Oct. 1953, pp. 657-674, 682.

5. Van Driest, E. R.; and Boison, J. Christopher: Experiments on Boundary-Layer Transition at Supersonic Speeds. J. Aeronaut. Sci., vol. 24, no. 12, Dec. 1957, pp. 885-899.

6. Laufer, John; and Marte, Jack E.: Results and a Critical Discussion of Transition-Reynolds-Number Measurements on Insulated Cones and Flat Plates in Supersonic Wind Tunnels. Rep. No. 20-96 (Contract No. DA-04-495-Ord 18), Jet Propul. Lab., California Inst. Technol., Nov. 30, 1955.

7. Pate, Samuel R.: Effects of Wind Tunnel Disturbances on Boundary-Layer Transition With Emphasis on Radiated Noise: A Review. AIAA-80-0431, Mar. 1980.

8. Stainback, P. C.; and Wagner, R. D.: A Comparison of Disturbance Levels Measured in Hypersonic Tunnels Using a Hot-Wire Anemometer and a Pitot Pressure Probe. AIAA Paper No. 72-1003, Sept. 1972.

9. Beckwith I. E.: Comments on Settling Chamber Design for Quiet, Blowdown Wind Tunnels. NASA TM-81948, 1981.

10. Morkovin, M. V.: On Supersonic Wind Tunnels With Low Free-Stream Disturbances. Trans. ASME, Ser. E: J. Appl. Mech., vol. 26, no. 3, Sept. 1959, pp. 319-324.

11. Wilkinson, Stephen P.; and Malik, Mujeeb R.: Stability Experiments in Rotating-Disk Flow. AIAA-83-1760, July 1983.

TABLE I.- PROFILOMETER DATA ON MACH 3.5 CONTOURED NOZZLE BLOCKS

[Typical sample 1/4 in. long across blocks; Stylus radius = 0.0001 in.]

Nozzle block	Axial distance,* in.	Lateral distance,** in.	Polish		rms finish, μin.		Roughness (peak to valley), μin.	
			Before polishing	After polishing	Typical range	Maximum local flaws	Typical	Maximum
1	0.250	9.026	x		6 to 10	10	50	70
				x	1 to 3	3	15	40
1	1.005	1.000	x		3 to 4	10	15	55
				x	1 to 3	3	8	15
2	.250	9.027	x		2	8	15	80
				x	1 to 2	2	15	20
2	1.005	1.000	x		2 to 3	25	25	100
				x	1 to 2	2	10	20
2	2.250	1.000	x		1 to 4	7 to 13	15	55
				x	1	5	10	15

*Axial distance downstream of lip.
**Lateral distance from edge of nozzle block.

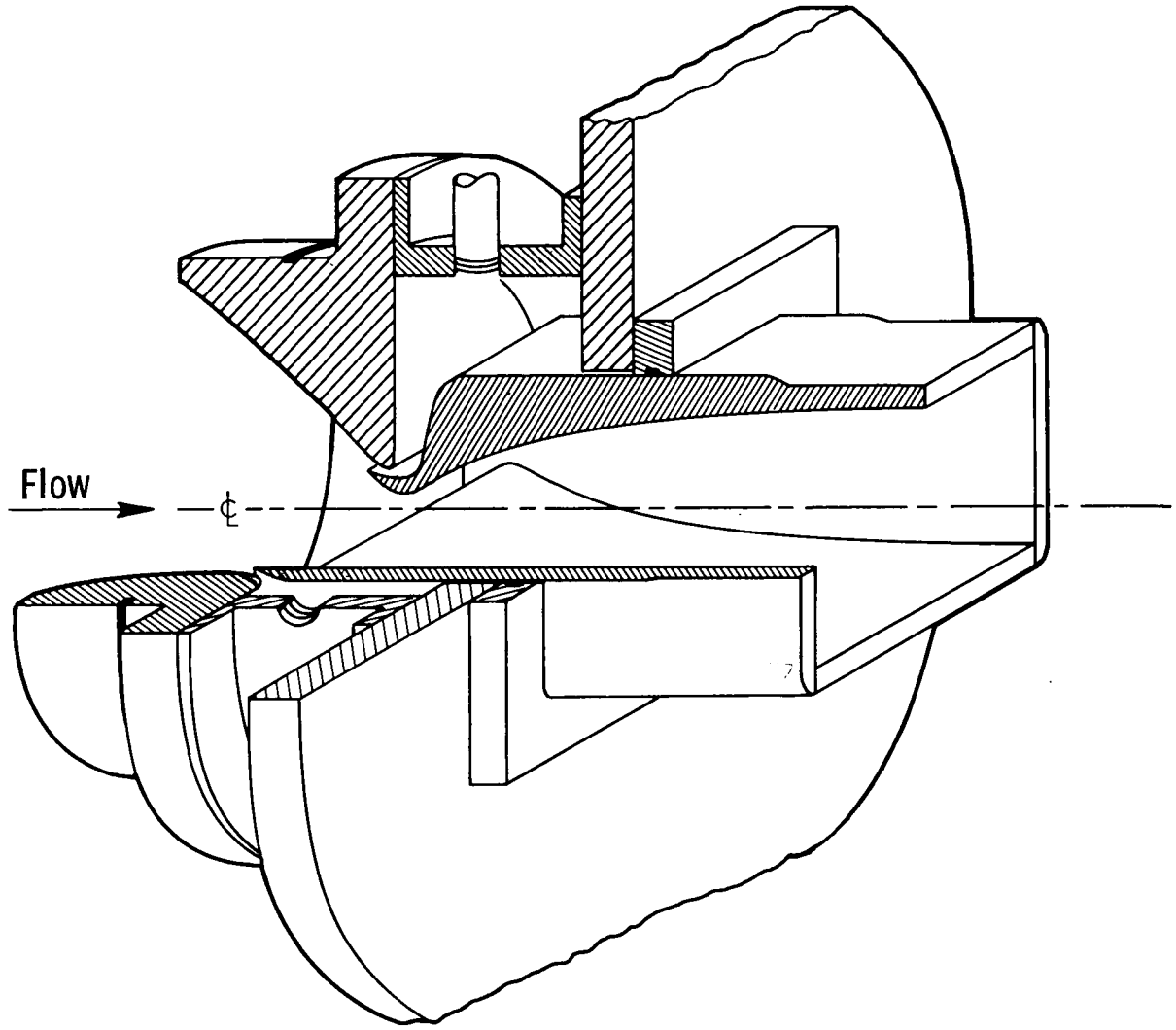

(a) Cutaway isometric sketch of boundary-layer bleed slots in subsonic approach and slot suction plenum. Throat = 0.898 by 10.025 in. wide; exit = 6.178 by 10.025 in. wide; throat-to-exit length = 15.467 in.

Figure 1.- Mach 3.5 two-dimensional nozzle.

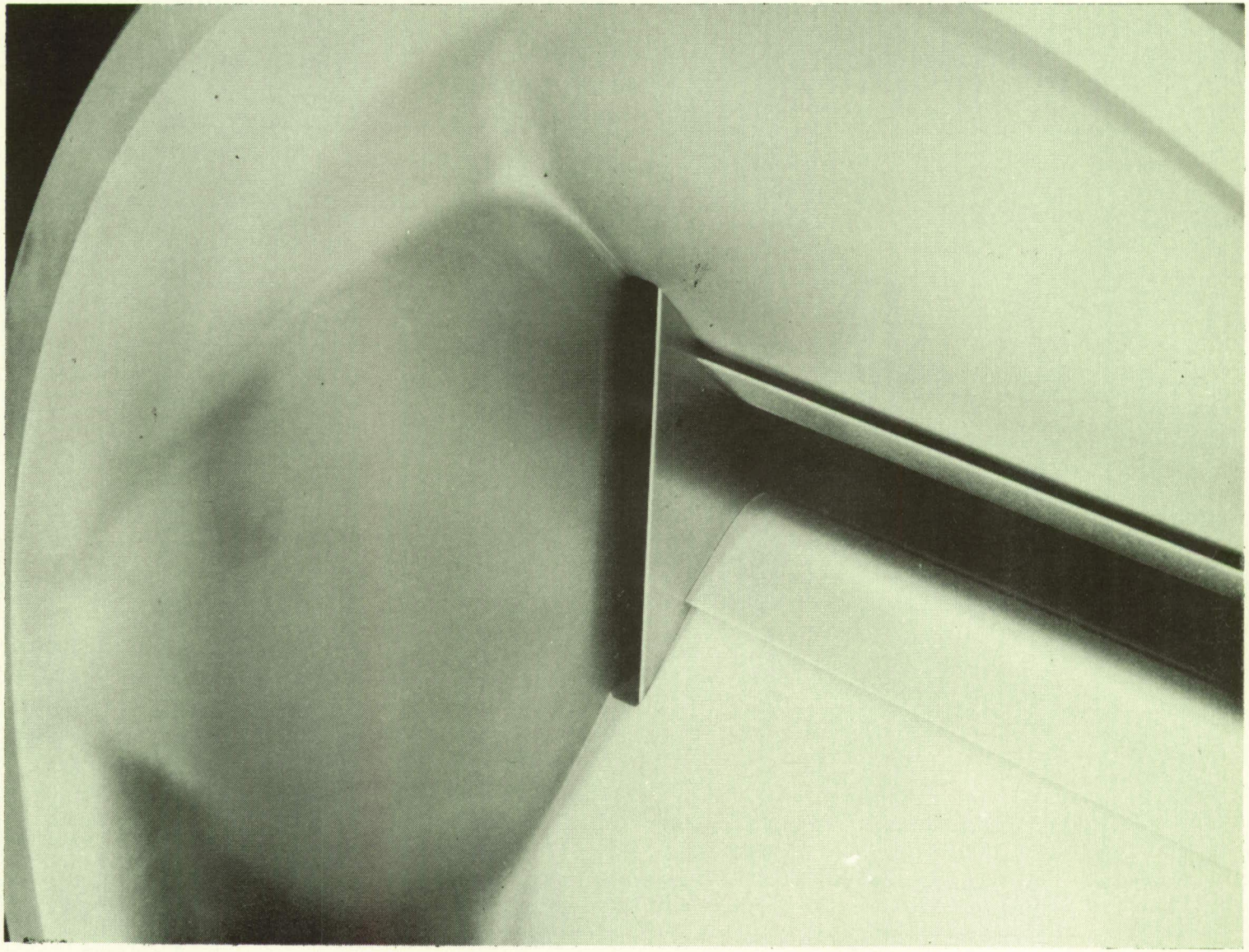

L-83-99

(b) Photograph of subsonic approach with details of sidewall and contour wall boundary-layer bleed slots.

Figure 1.- Concluded.

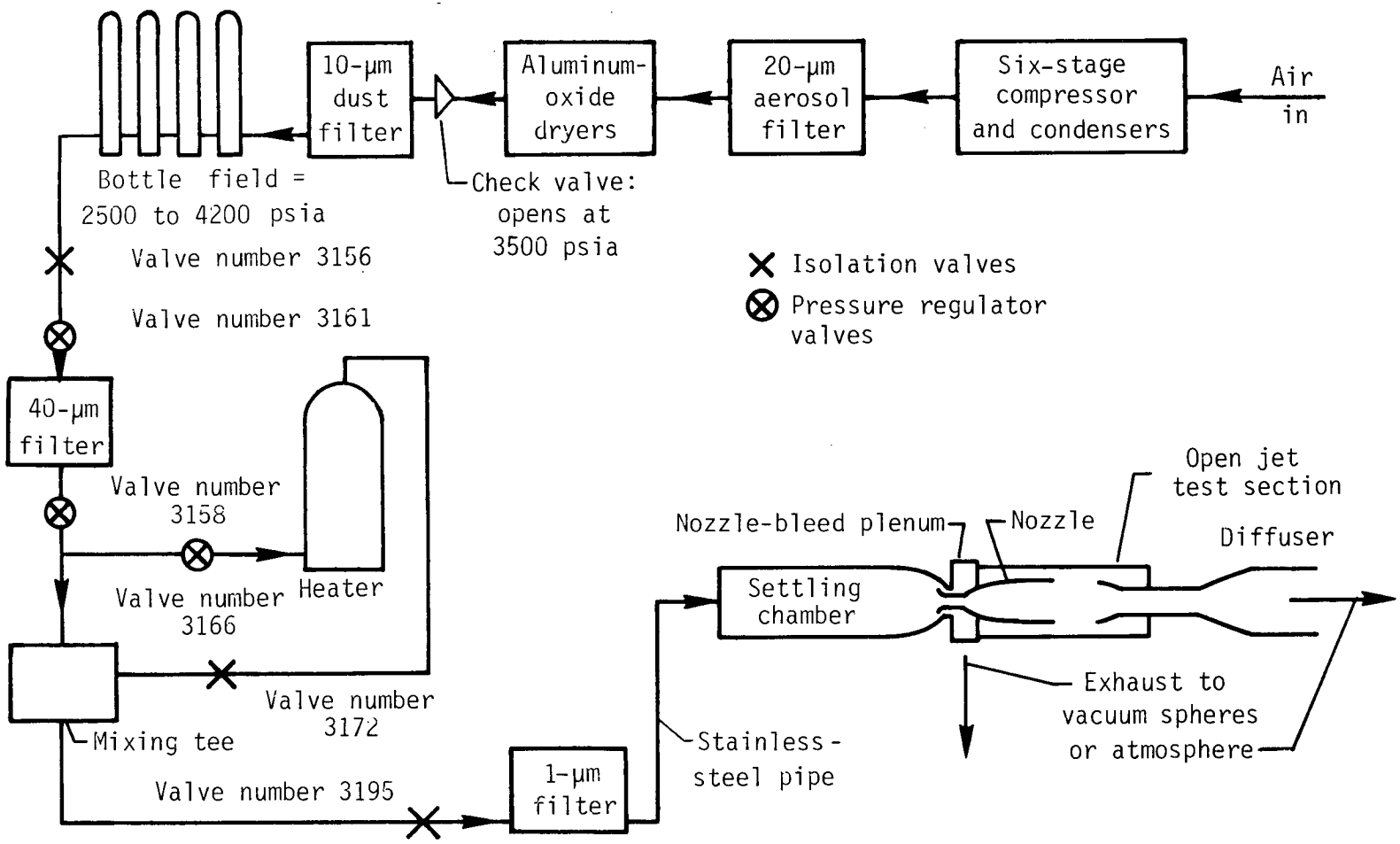

Figure 2.- Schematic sketch of pilot low-disturbance tunnel air supply system.

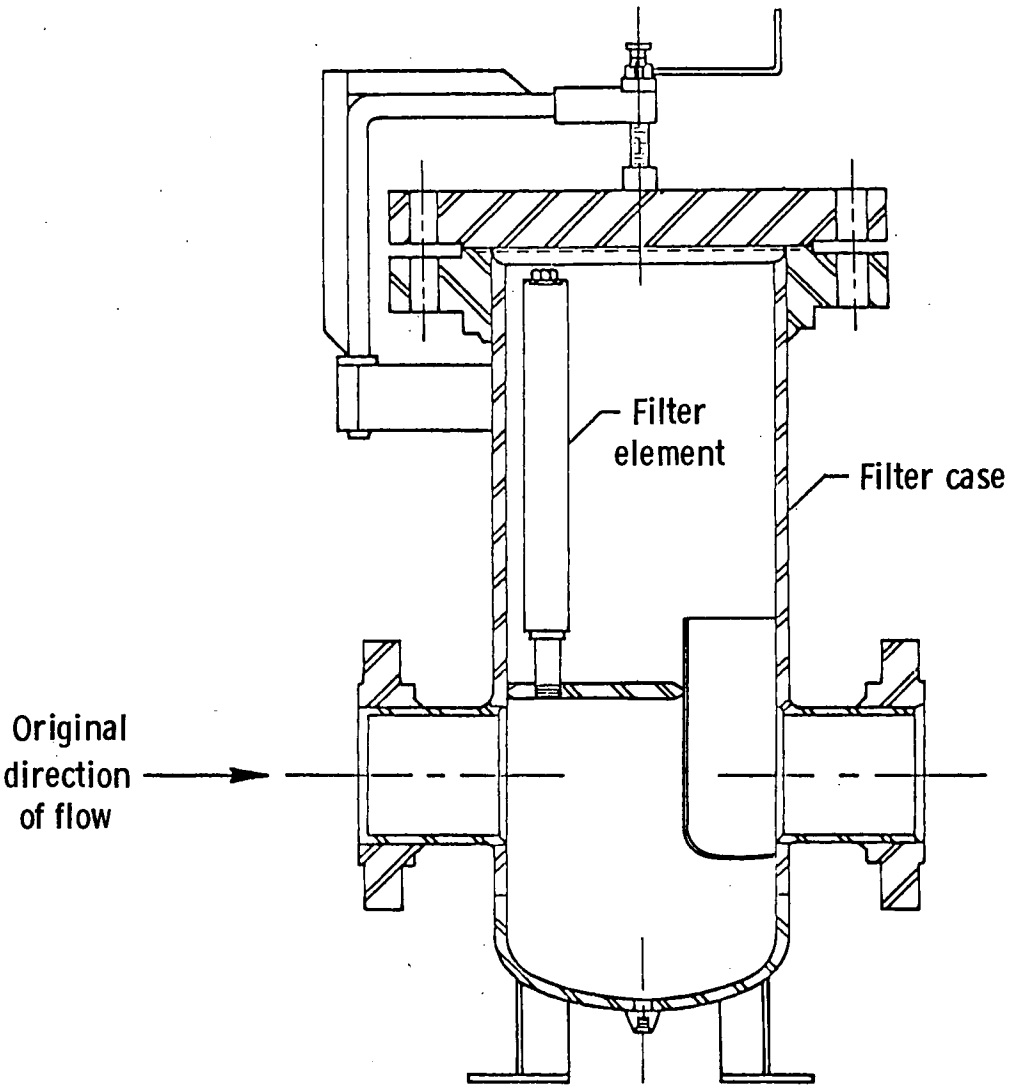

(a) Side view.

Figure 3.- Sectional drawings of the final air supply filter.

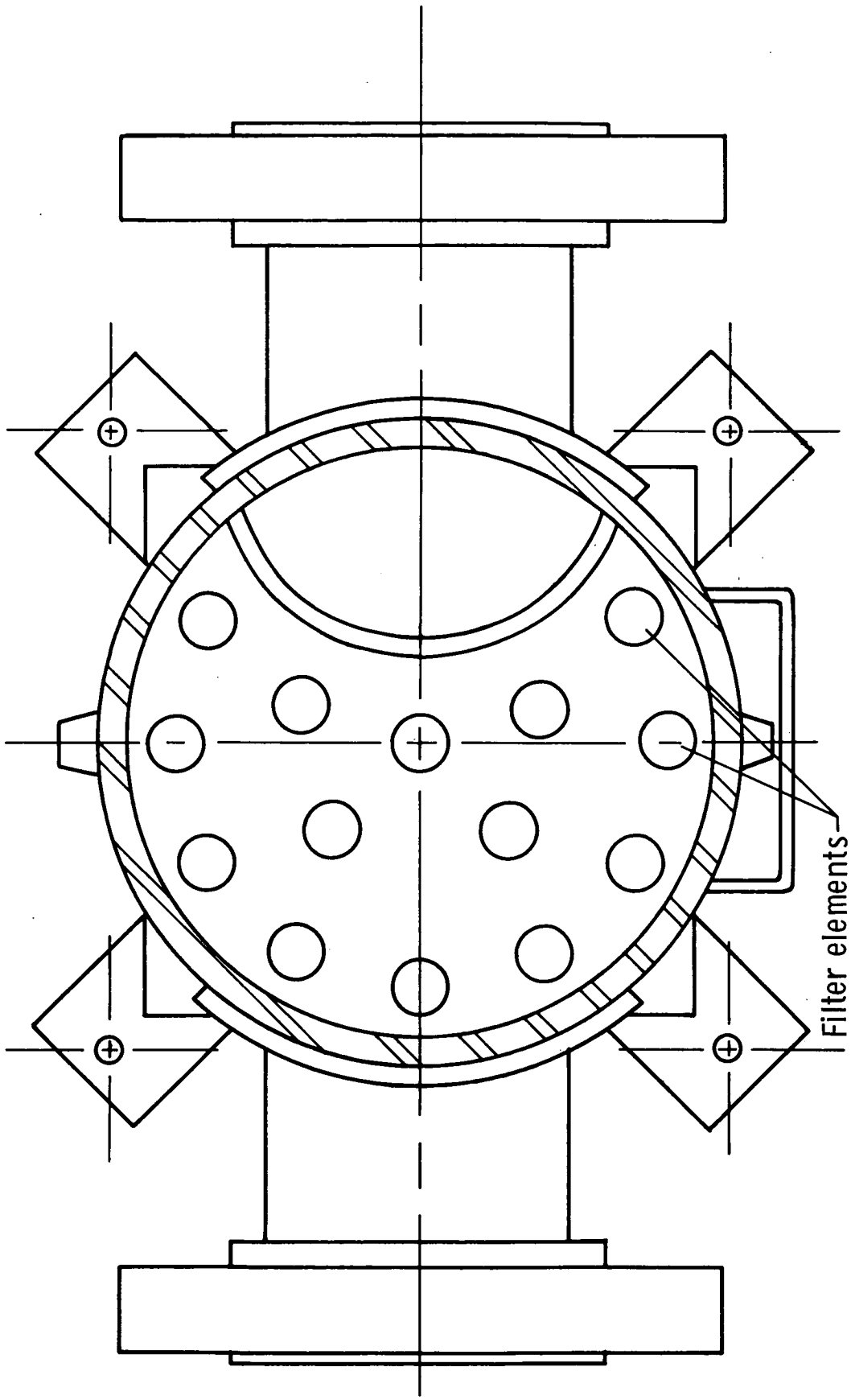

(b) Top view.

Figure 3.- Concluded.

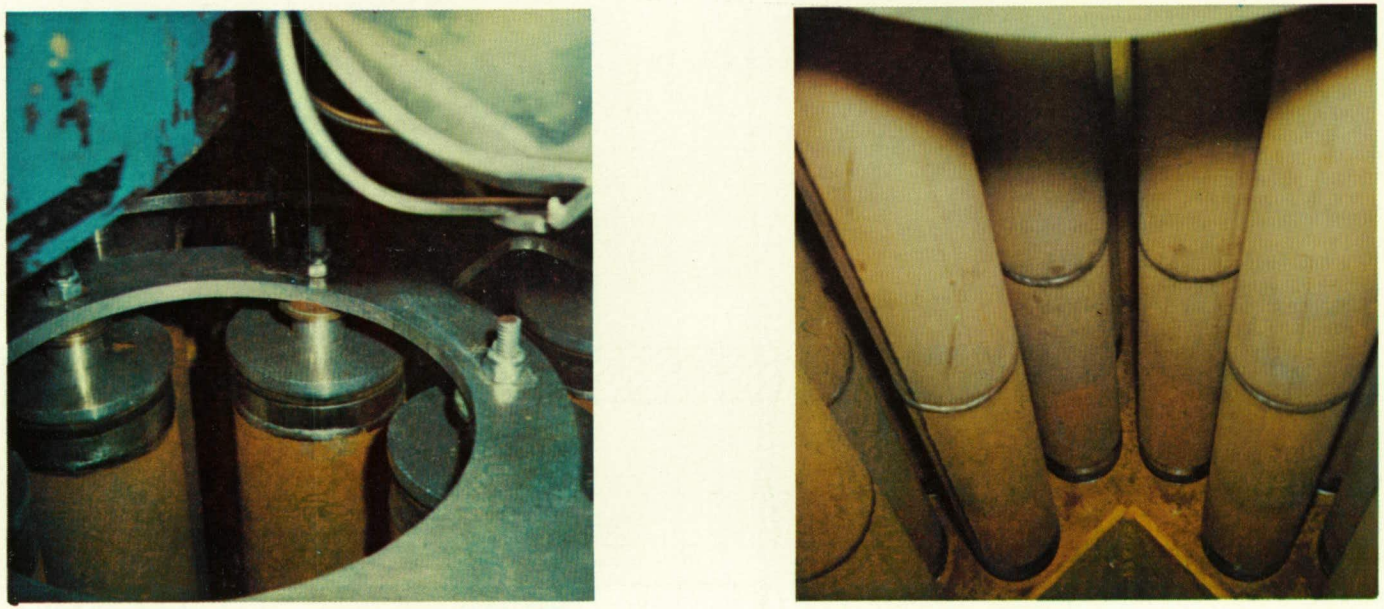

(a) Top.

(b) Bottom.

L-85-70

Figure 4.- Inside of filter with contaminated stainless-steel elements with flat gaskets (fig. 5(a)).

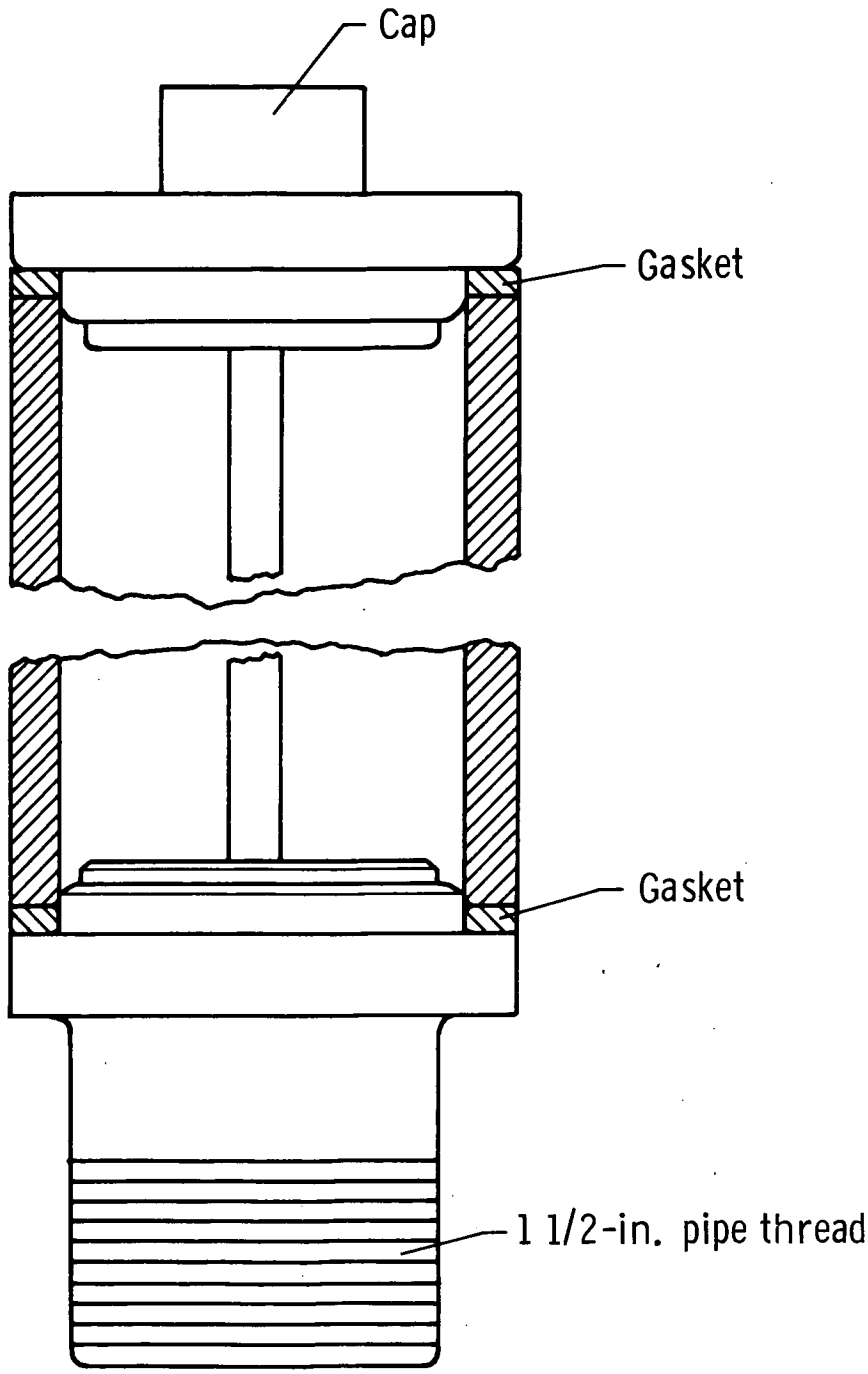

(a) Element arrangement with flat gaskets.

Figure 5.- Stainless-steel filter element.

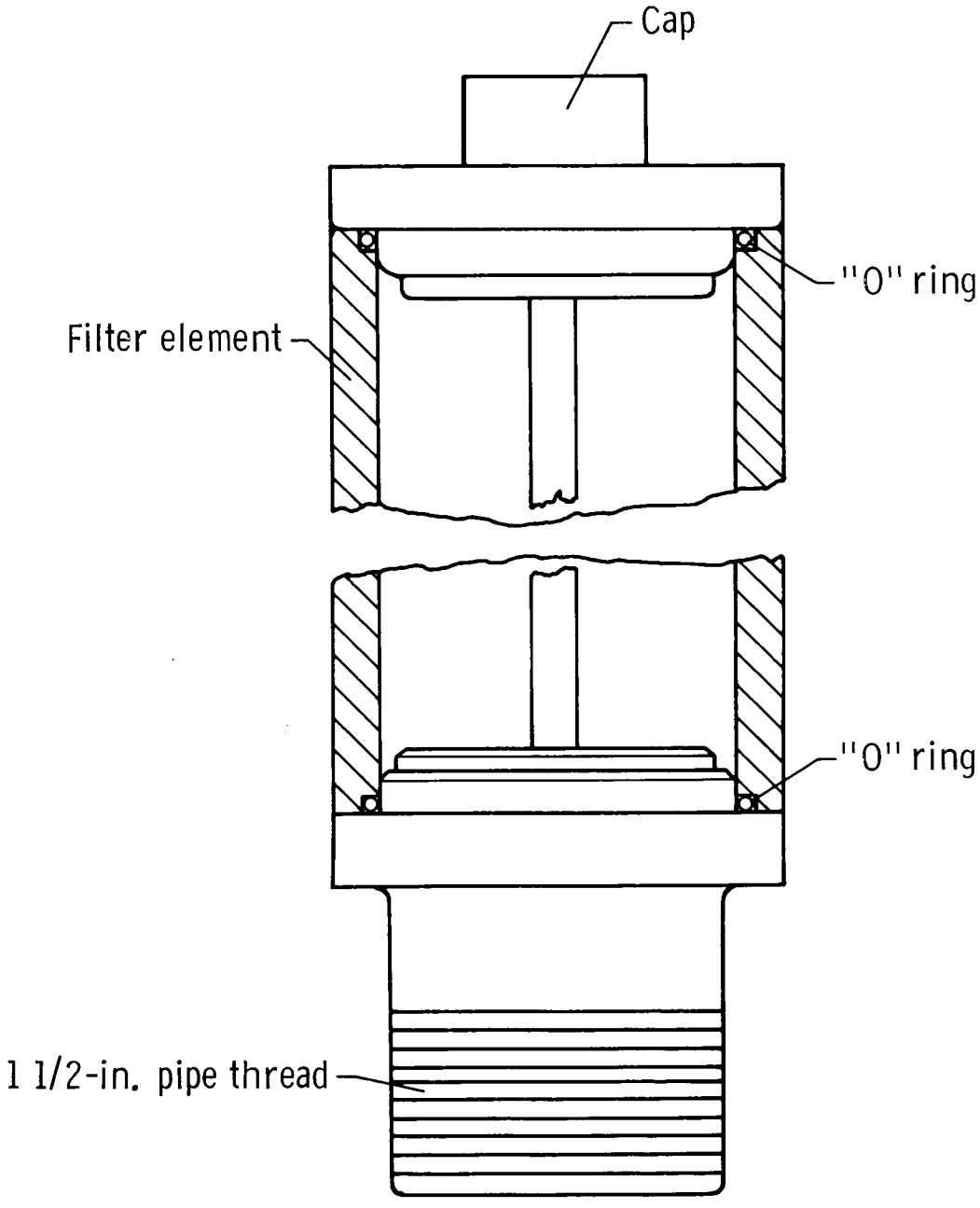

(b) Element arrangement with O-ring seals.

Figure 5.- Continued.

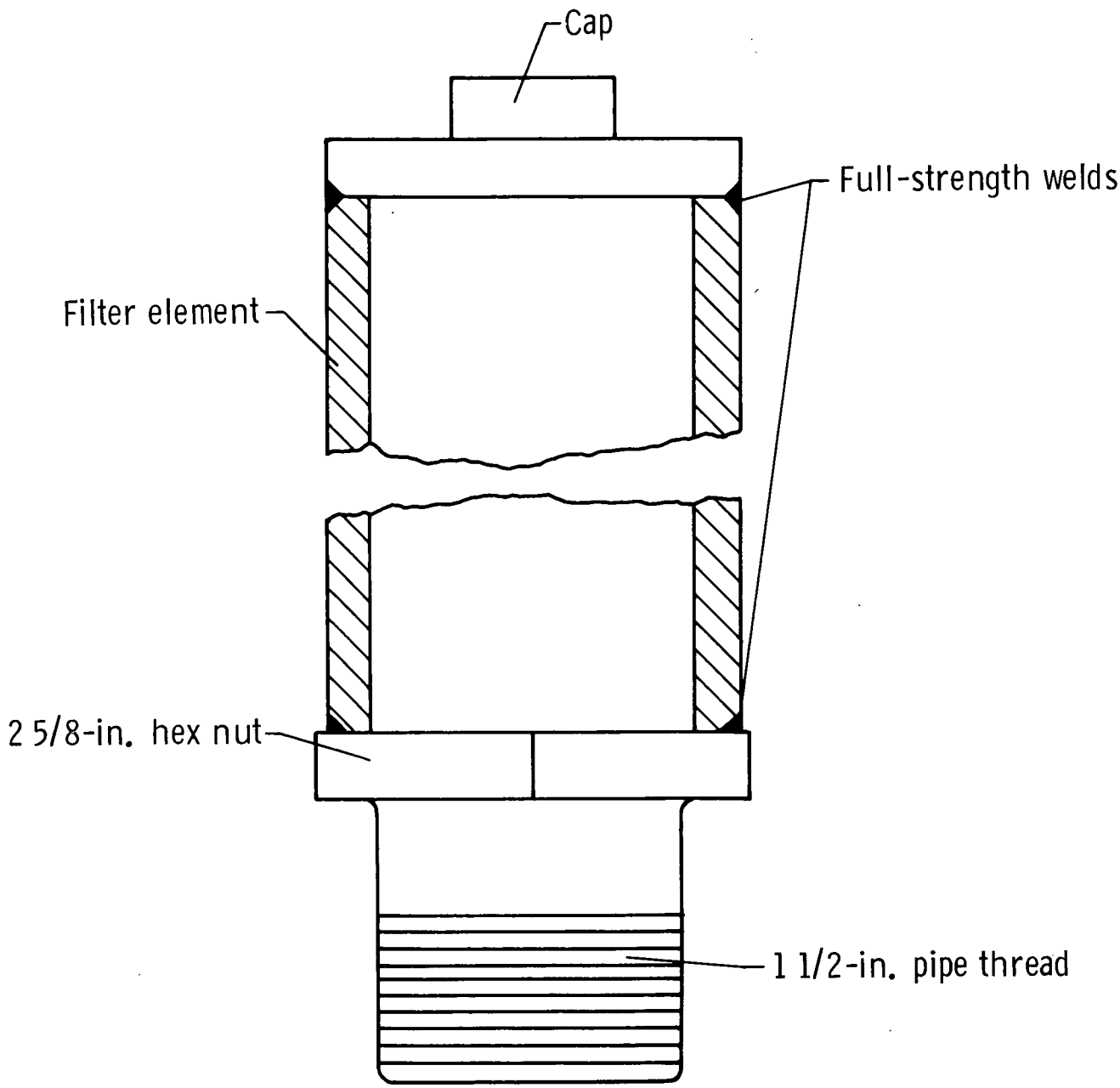

(c) Final filter element with welded end caps.

Figure 5.- Concluded.

L-85-71

(a) Black dust.

Figure 6.- Typical sample of the flow contaminants in the pilot low-disturbance tunnel free stream before the porous stainless-steel filter elements were installed. Enlargement = 150 x.

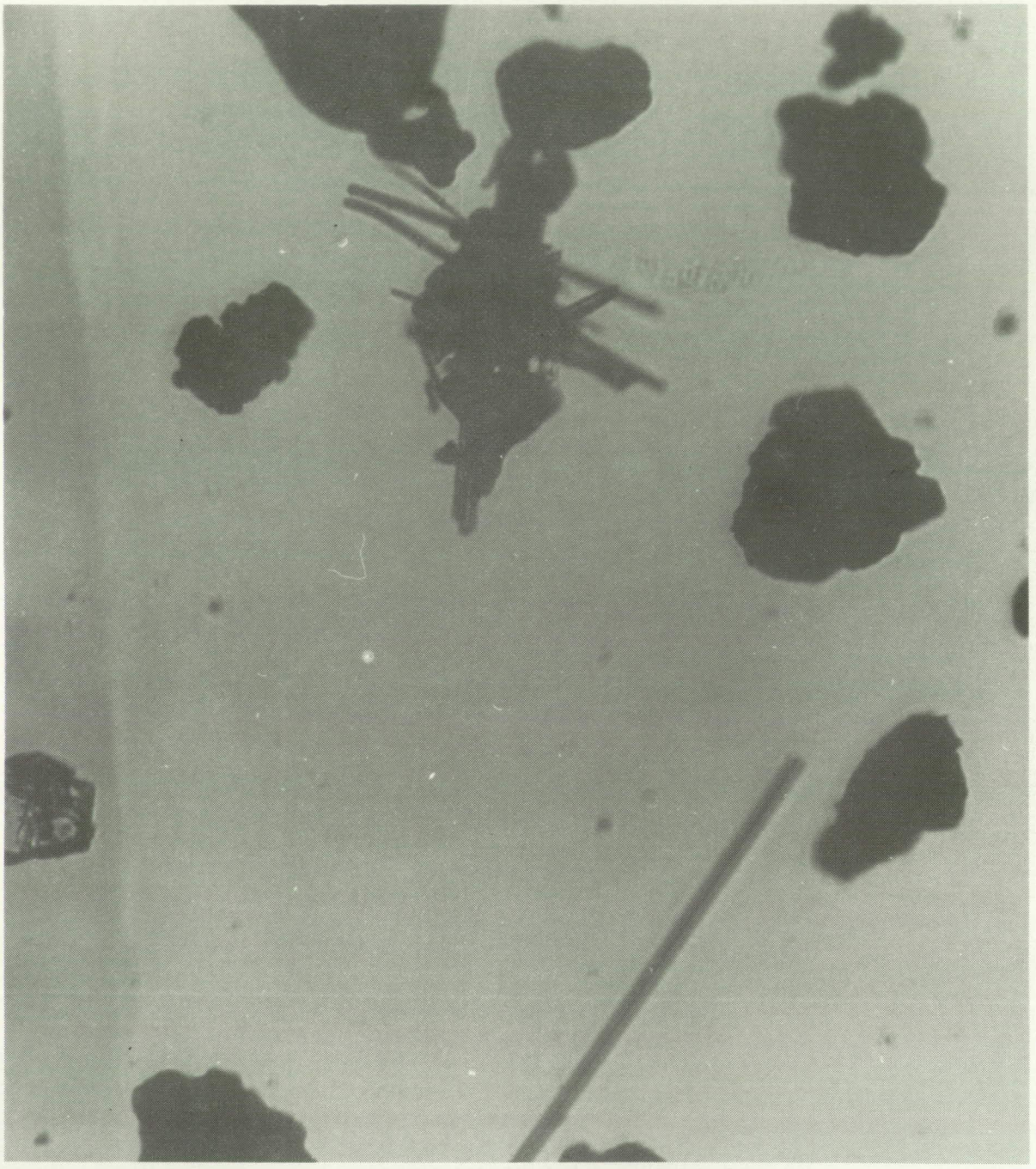

L-85-72

(b) Small fibers.

Figure 6.- Concluded.

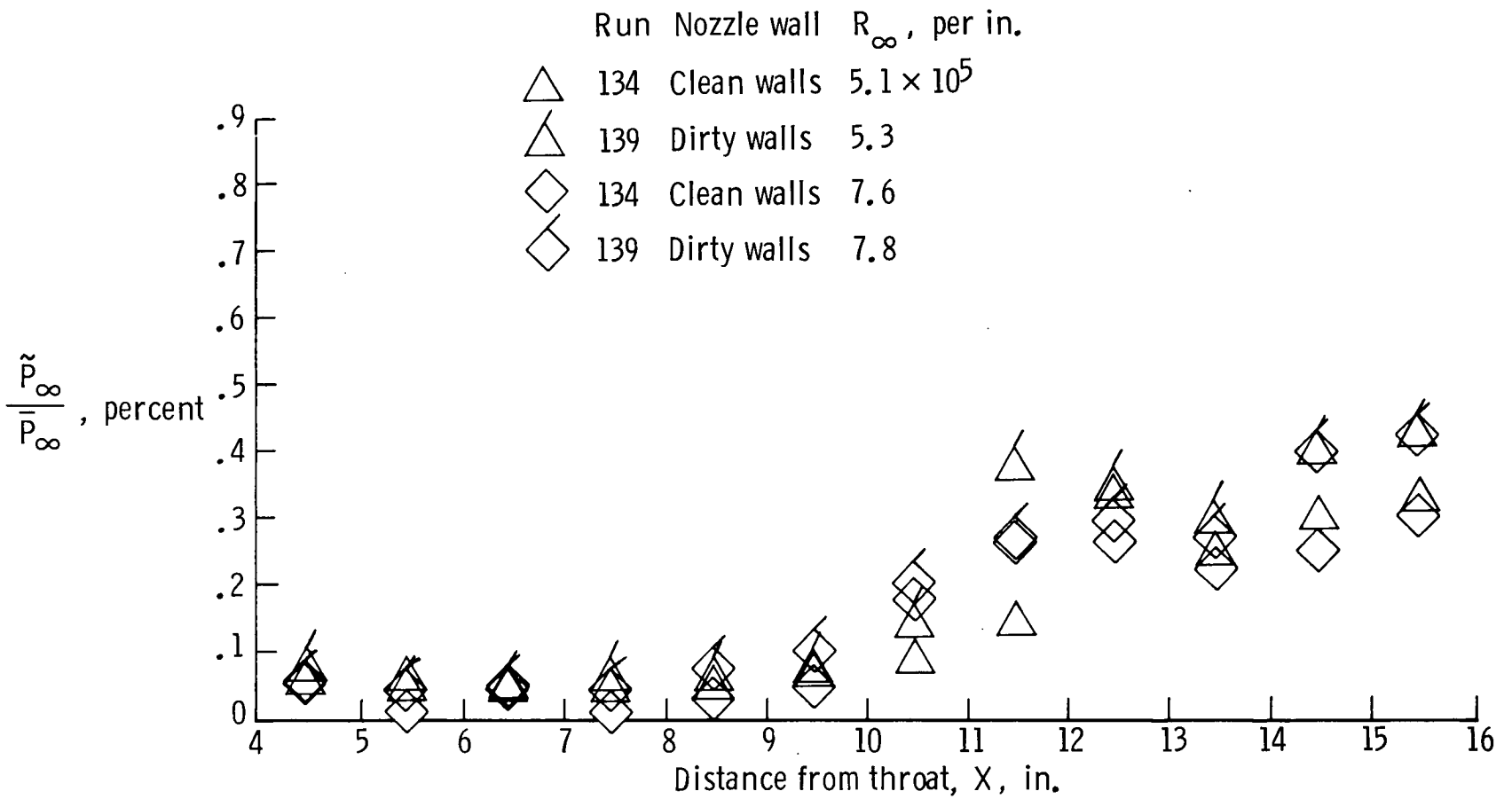

(a) $5.1 \times 10^5 \leq R_\infty \leq 7.8 \times 10^5$ per in.

Figure 7.- Effects of dust deposits on normalized rms static pressure on nozzle centerline. Bleed valve open.

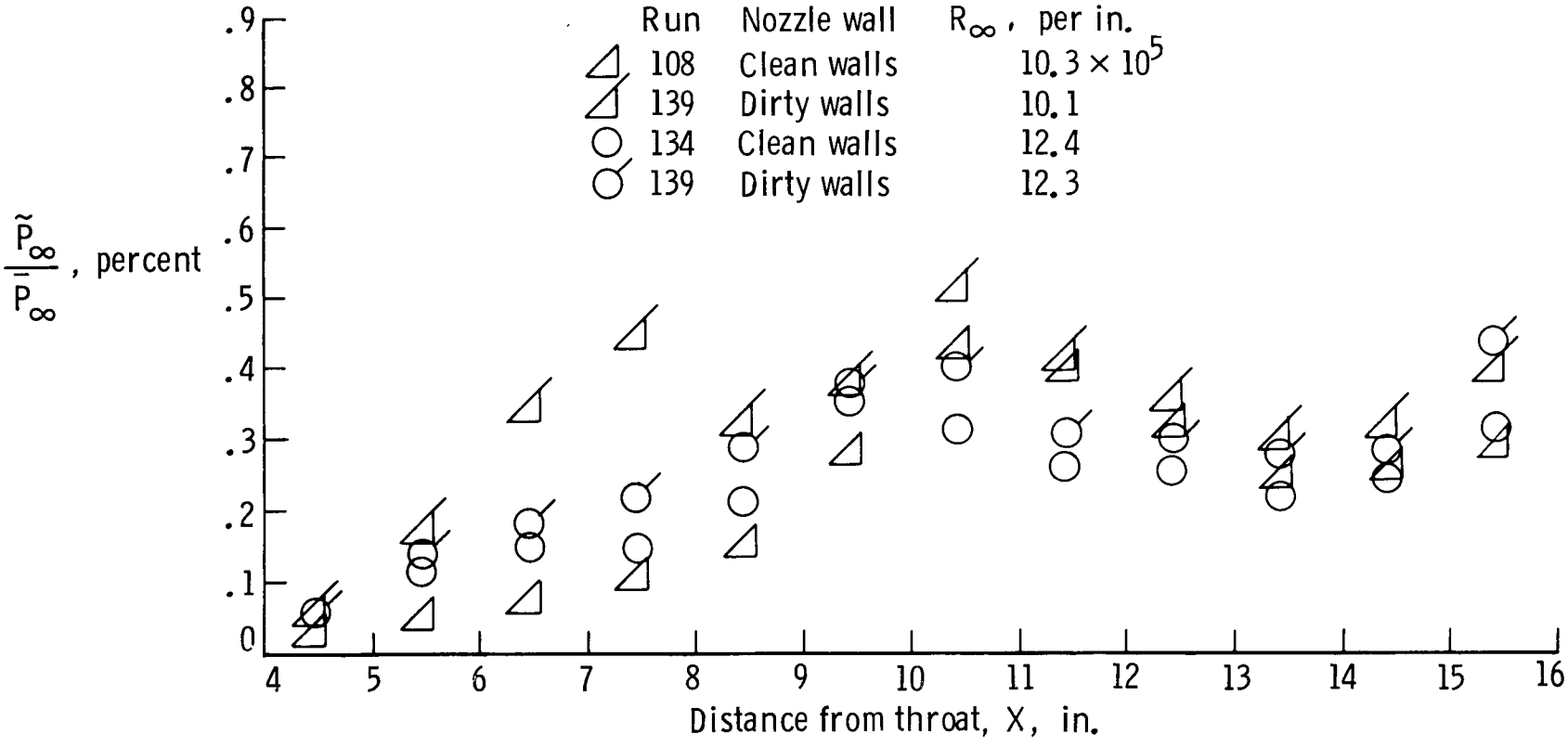

(b) $10.1 \times 10^5 \leq R_\infty \leq 12.4 \times 10^5$ per in.

Figure 7.- Concluded.

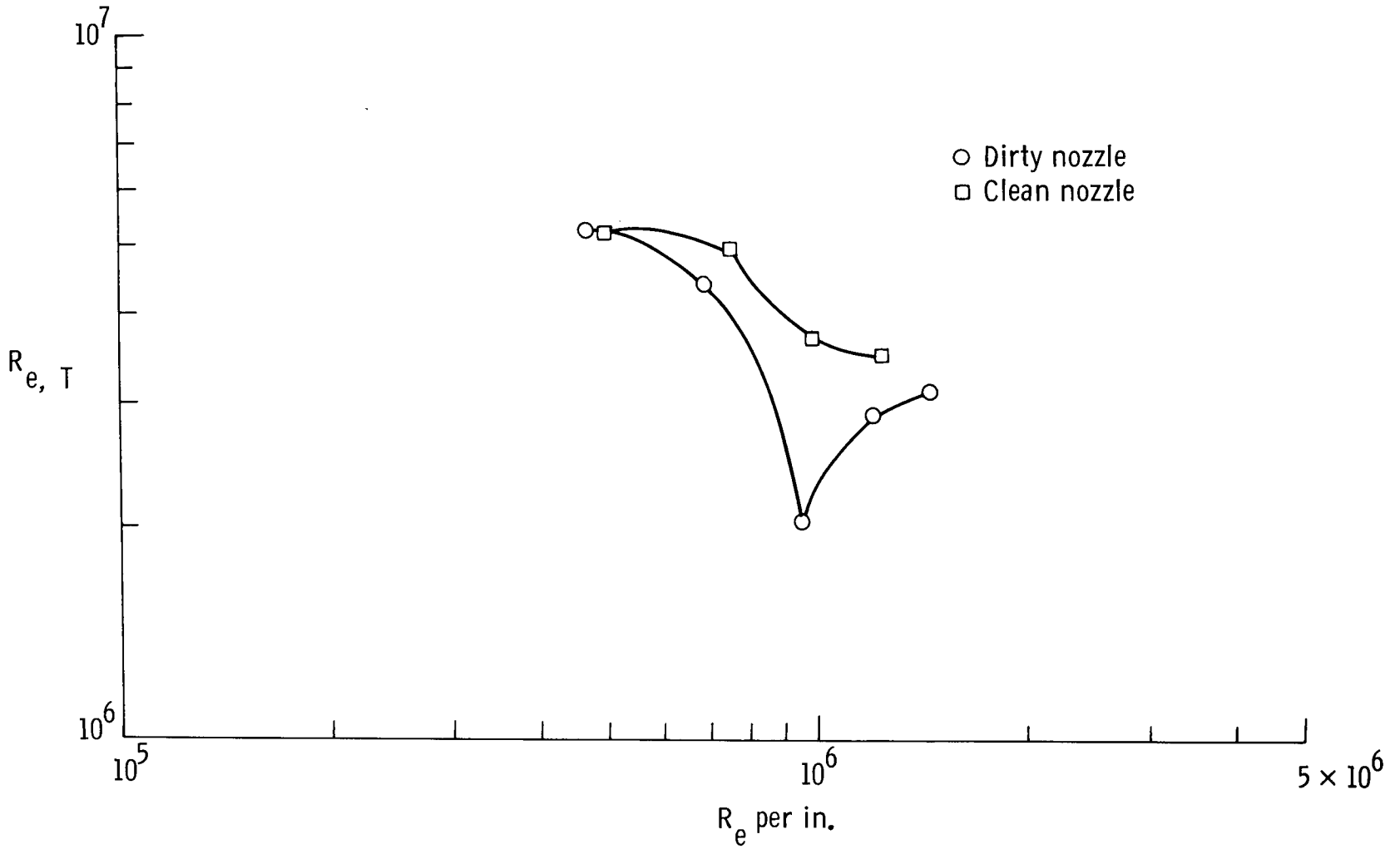

Figure 8.- Nozzle contamination effects on transition Reynolds numbers on cone 1. X_c = 8 in. Bleed valve open.

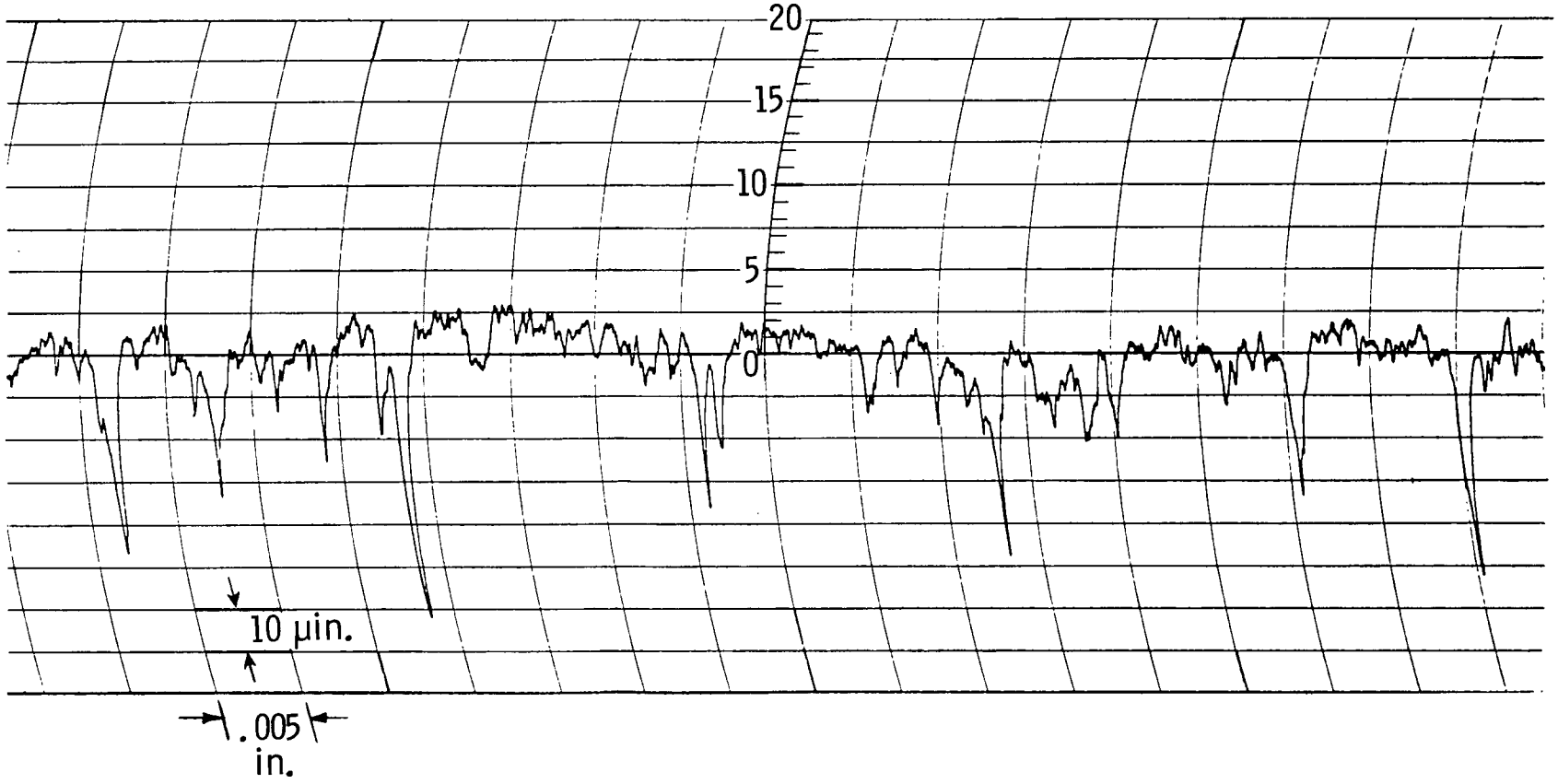

(a) Before surface repolishing.

Figure 9.- Profilometer traces of nozzle surface roughness.
Axial direction = 0.250 in. from nozzle lip. Width distance = 9.026 in.
from nozzle side wall.

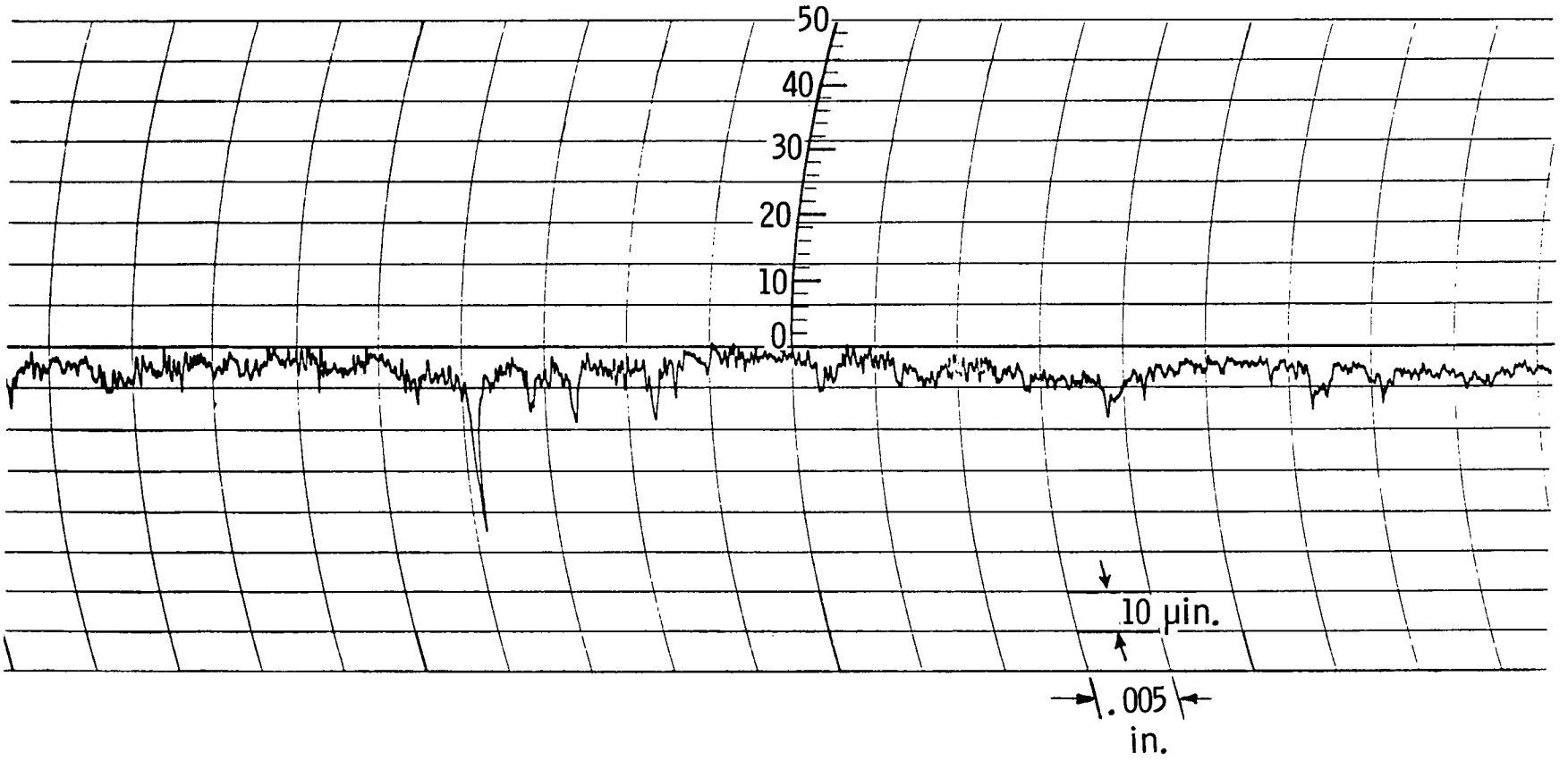

(b) After surface repolishing.

Figure 9.- Concluded.

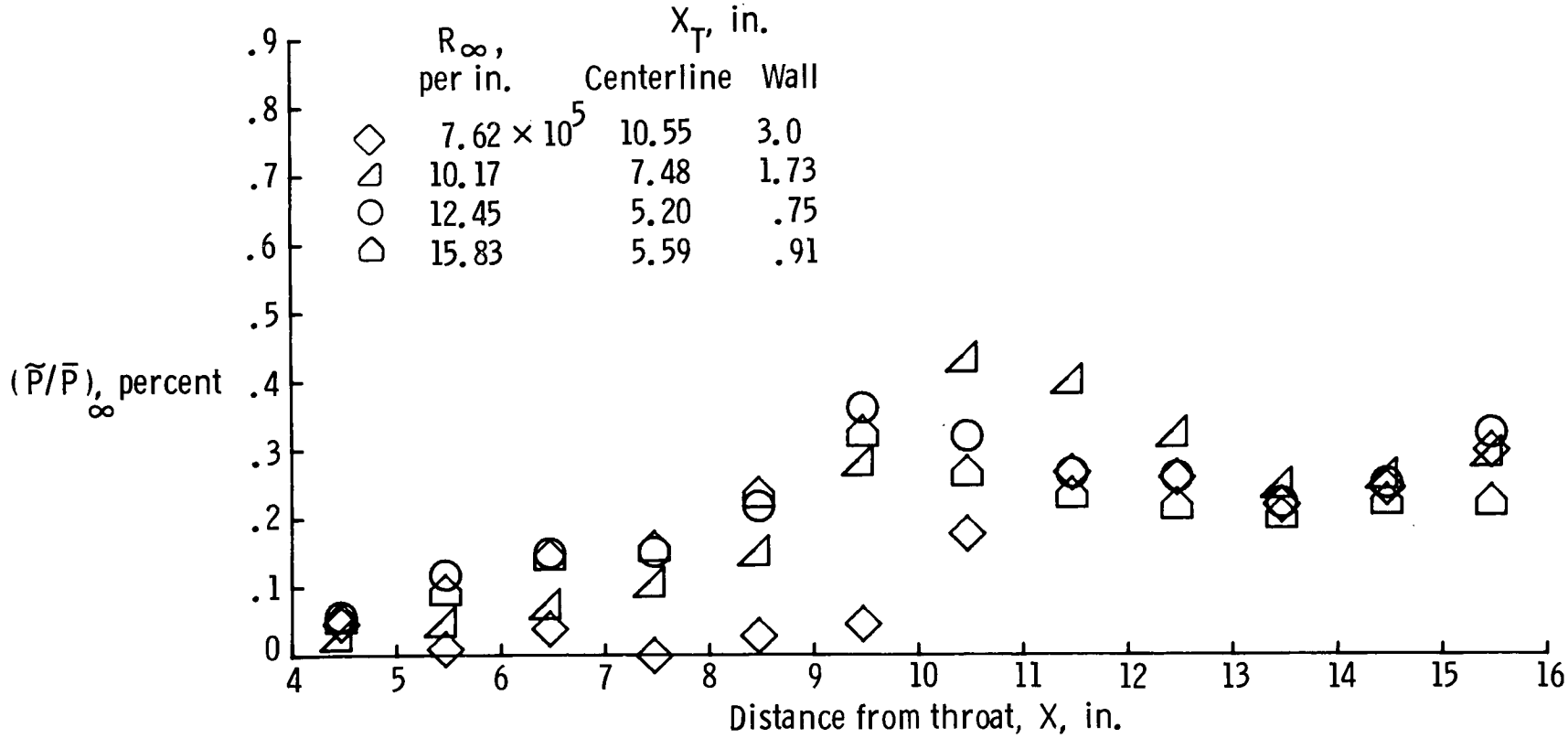

(a) Before repolishing. Hot-wire data from reference 1.

Figure 10.- Variation in normalized rms pressure along centerline of Mach 3.5 pilot nozzle.

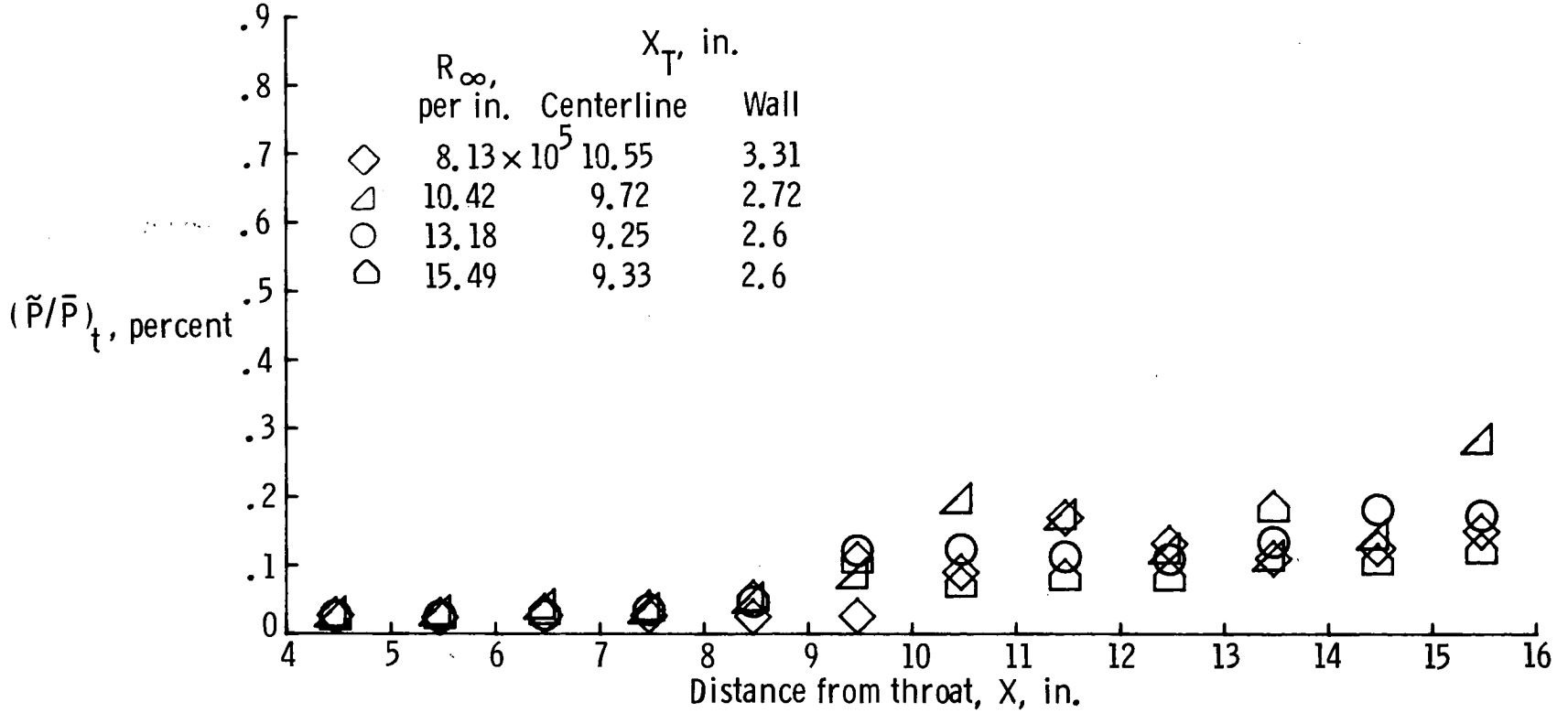

(b) After repolishing. New data from fluctuating pitot pressure probe.

Figure 10.- Concluded.

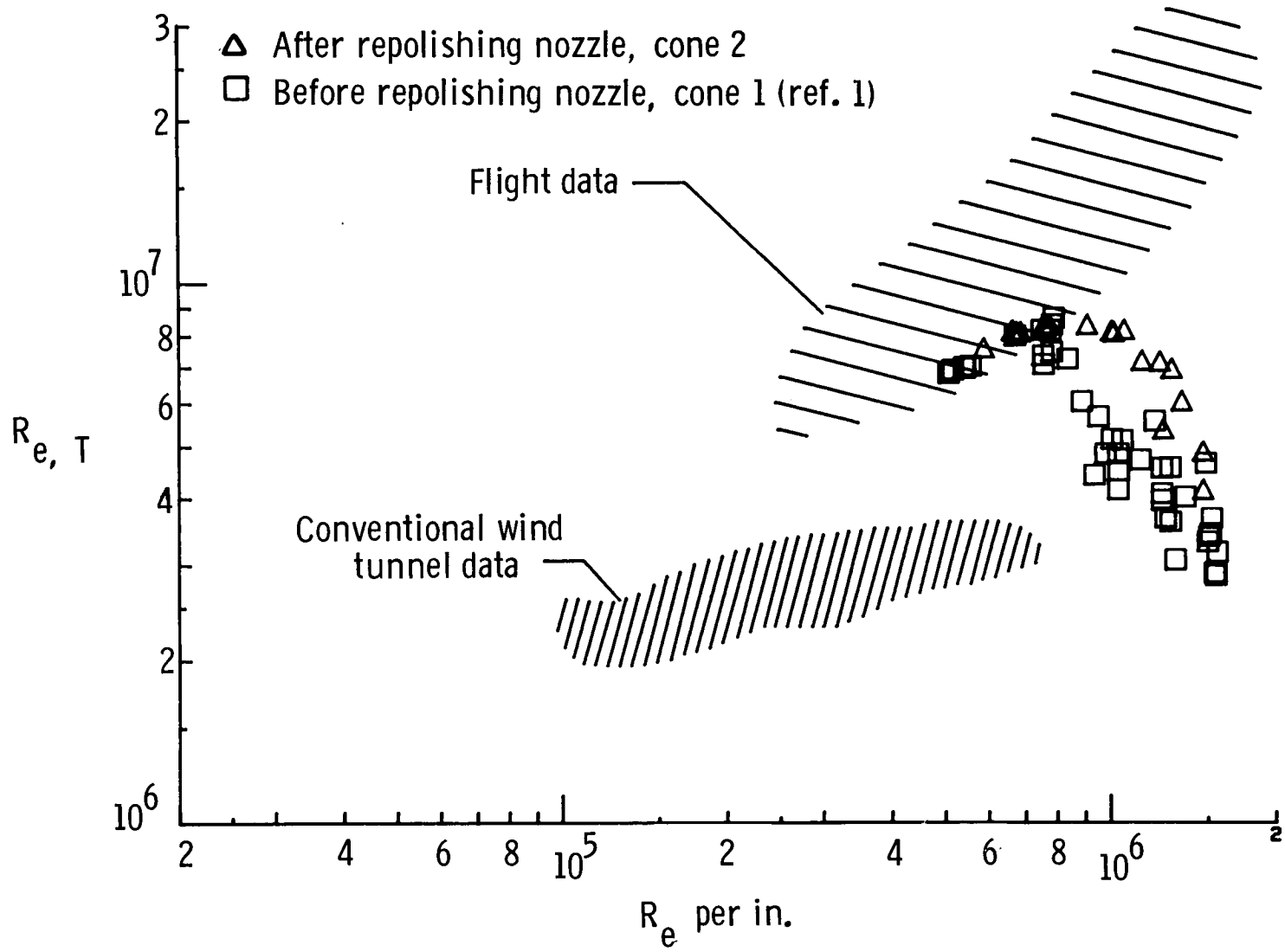

(a) Bleed valve open.

Figure 11.- Variation of transition Reynolds number with unit Reynolds number on sharp-tip cones in Mach 3.5 pilot low-disturbance tunnel. Cone tip at 5 in. from nozzle throat.

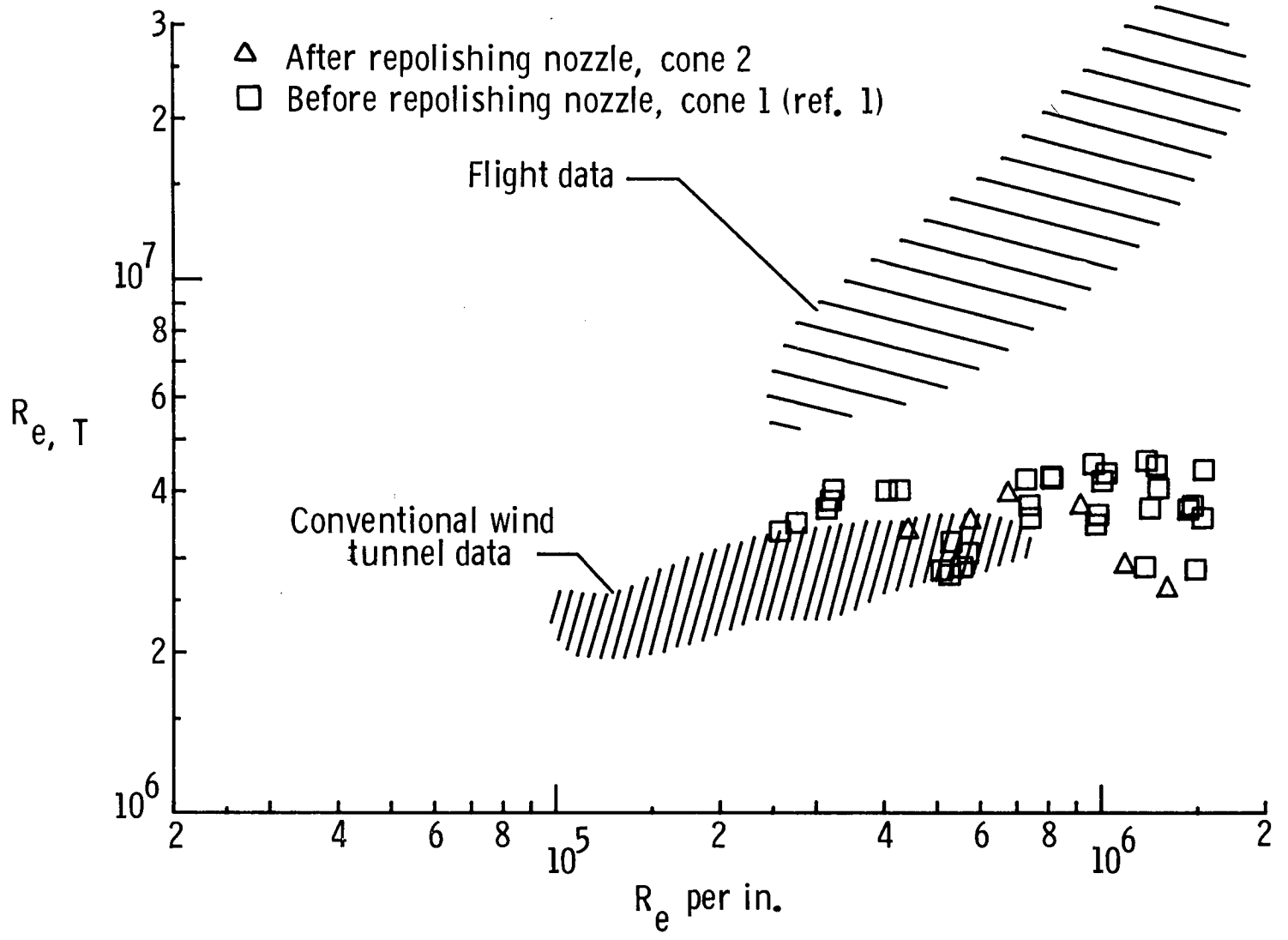

(b) Bleed valve closed.

Figure 11.- Concluded.